Mobile Communications Beyond 52.6 GHz: Waveforms, Numerology, and Phase Noise Challenge

Toni Levanen, Oskari Tervo, Kari Pajukoski, Markku Renfors, and Mikko Valkama

***Abstract*—In this article, the 5G New Radio (NR) physical layer evolution to support beyond 52.6 GHz communications is addressed. The performance of both OFDM based and DFT-s-OFDM based networks are evaluated with special emphasis on the phase noise (PN) induced distortion. It is shown that DFT-s-OFDM is more robust against PN under 5G NR Release 15 assumptions, specifically regarding the supported phase tracking reference signal (PTRS) designs. To further improve the PN compensation capabilities, the PTRS design for DFT-s-OFDM is revised, while for the OFDM waveform a novel block PTRS structure is introduced, providing similar link performance as DFT-s-OFDM with enhanced PTRS design. We demonstrate that the existing 5G NR Release 15 solutions can be extended to support deployments at 60 GHz bands with the enhanced PTRS structures. In addition, DFT-s-OFDM based downlink for user data could be considered for beyond 52.6 GHz communications to further improve system power-efficiency and performance with higher order modulation and coding schemes. Finally, network link budget and cell size considerations are provided, showing that at certain bands with specific transmit power regulation, the cell size can eventually be downlink limited.**

***Index Terms*—5G evolution, 5G New Radio, beyond 52.6 GHz, DFT-s-OFDM, link budget, numerology, OFDM, phase noise, phase tracking reference signal, physical layer**

I. Introduction

The frequencies beyond 52.6 GHz contain very large spectrum opportunities and will thus facilitate many high capacity use cases, as envisioned in [1]. Operation at the millimeter waves (mmWaves) has, however, many differences compared to the lower frequencies [2], [3]. The severely increased path loss (PL) implies that directional antenna arrays with large number of antenna elements are needed. Beam-based operation with narrow beams results in more complex channel access mechanisms, more exhaustive beam training and refinement procedures, and mainly line-of-sight (LOS) communications. Another major factor is the decreased power efficiency of power amplifiers (PAs). Specifically, PAs operating at mmWaves have typically lower output powers while being also more non-linear compared to the more traditional PAs at lower frequencies [4], implying decreased system power efficiency and coverage. It is also well-known that orthogonal frequency division multiplexing (OFDM) signals have larger peak-to-average-power ratio (PAPR) than discrete Fourier transform (DFT) spread OFDM (DFT-s-OFDM) [2], especially at lower modulation orders. Thus supporting DFT-s-OFDM in both downlink (DL) and uplink (UL) in the beyond 52.6 GHz networks is important for enhanced coverage and power efficiency – an issue that is addressed in this article.

Another important implementation challenge at mmWaves is the oscillator phase noise (PN). Already in the 3GPP Release 15 (Rel-15) of 5G New Radio (NR) [3], [5], [6], the so-called phase tracking reference signals (PTRSs) were defined, which allow the receiver (RX) to estimate and compensate the PN effects. However, as PN increases for increasing carrier frequency [7], the current solutions may not be sufficient to guarantee good performance in beyond 52.6 GHz communications – an aspect that is explicitly addressed in this article.

In this paper, after some considerations on the available bands for beyond 52.6 GHz networks, the evolution of the physical layer (PHY) numerology in terms of subcarrier spacing (SCS), slot duration and potential channel bandwidths is addressed. Then, the important oscillator PN challenge is studied, with specific emphasis on new and novel PTRS structures. This is followed by radio link performance evaluations at 60 GHz, considering both OFDM and DFT-s-OFDM, where the envisioned new PHY numerologies as well as the different PTRS designs are deployed, while also comparing against the Rel-15 NR based network. It is shown that DFT-s-OFDM is more robust against PN distortion and can operate with smaller SCS than OFDM, especially with higher modulation orders. This is due to the time-domain group-wise PTRS design of DFT-s-OFDM, which allows to track the time-varying PN realization within a DFT-s-OFDM symbol. We also show that DFT-s-OFDM based radio link performance can be further improved by designing new PTRS configurations with only modest increase in the PTRS overhead. In addition, to improve the OFDM performance, a novel block PTRS design is devised, allowing to nearly achieve the DFT-s-OFDM link performance. Finally, the cell-size and the associated UL/DL link budget aspects are addressed, considering both OFDM and DFT-s-OFDM, while also comparing PA technology limited and EIRP limited systems. It is shown that at EIRP limited bands, the network coverage may actually be downlink limited.

II. Spectrum Prospects at Beyond 52.6 GHz Bands

The current spectrum availability between 52.6 GHz and 100 GHz [1] is illustrated at high level in Table I. Regarding the unlicensed access based mobile communications, global spectrum is available at 59 GHz–64 GHz. Furthermore, the best availability is in USA, where the wide frequency range of 57 GHz–71 GHz is providing a total bandwidth of 14 GHz.

T. Levanen, M. Renfors, and M. Valkama are with Department of Electrical Engineering, Tampere University, Finland (firstname.lastname@tuni.fi)

O. Tervo and K. Pajukoski are with Nokia Bell Labs, Oulu, Finland (firstname.lastname@nokia-bell-labs.com)

This article contains supplementary electronic materials, available at IEEE-Xplore and at https://research.tuni.fi/wireless/research/WCM2020B50GHz/

TABLE I: Current spectrum availability in various countries between frequencies 52.6 GHz and 100 GHz [1], including indicators for unlicensed (U) or licensed (L) spectrum access and for allowed use cases of mobile (M) or fixed (F) point-to-point communications.

Country/Region	**Frequency [GHz]**												
	52.6-57	57-59	59-64	64-66	66-71[1)]	71-76	76-81	81-86	86-92	92-94	94-94.1	94.1-95	95-100
Europe		U;M			U/L;M	L;F		L;F		L;F			
South Africa		U;M			U/L;M	L;F		L;F					
USA		U;M				L;F/M		L;F/M		L;F/M		L;F/M	
Canada		U;M			U/L;M	L;F		L;F					
Brazil		U;M			U/L;M	L;F		L;F					
Mexico		U;M			U/L;M	L;F		L;F					
China			U;M		U/L;M								
Japan		U;M			U/L;M	L;F		L;F					
Singapore		U;M			U/L;M	L;F		L;F					
1) Allowed for administrations wishing to implement the terrestrial component of IMT, by RESOLUTION COM4/7 (WRC-19).													

As there are uncertainties when the other beyond 52.6 GHz bands are available for mobile communications, there is a strong motivation to study the extension of the current Rel-15 solutions to operate also at 57 GHz – 71 GHz, commonly called the 60 GHz band(s). It should be highlighted, however, that the direct extension of current Rel-15 operation is not a suitable long term solution when aiming to cover a wider range of carrier frequencies beyond 52.6 GHz. Up to now, the upper limit of the 3GPP studies has been 114.25 GHz [1], but even higher carrier frequencies could be envisioned in the near future, and thus a study on a new common waveform for beyond 52.6 GHz communications is of large interest.

In general, the frequencies above 71 GHz are mainly reserved for fixed, point-to-point communications, except in USA where both mobile and fixed communications are allowed. Considering the regulation in Europe for 71 GHz – 100 GHz, up to 18 GHz aggregated licensed bandwidth is available for fixed communications. If these frequencies were available in mobile communications, the larger channel bandwidths envisioned in Section III could be directly deployed.

III. 5G NR Physical Layer: Current Status and Beyond 52.6 GHz Evolution

A. Physical Layer Numerology of 5G NR Rel-15

The supported SCSs of 5G NR Rel-15 follow the scaling of 15 kHz with powers of two, defined as $15\times 2^{\mu}$ kHz, where $\mu \in \{0, 1, 2, 3, 4\}$, corresponding to SCSs of 15/30/60/120/240 kHz [5]. The frequency range 1 (FR1) is defined for carrier frequencies 410 MHz – 7.125 GHz and supports SCSs of 15/30/60 kHz, while the FR2 defined for 24.25 GHz – 52.6 GHz supports 60/120/240 kHz SCSs, where 240 kHz SCS is only allowed for the so-called synchronization signal block [6]. The 5G NR Rel-15 related main PHY parameters are summarized in Table II. Finally, Rel-15 supports OFDM in DL while both OFDM and DFT-s-OFDM in UL.

B. Physical Layer Numerology for Beyond 52.6 GHz Evolution

The current Rel-15 specification does not provide sufficient flexibility and power-efficiency for communications above 52.6 GHz bands. Specifically, in beyond 52.6 GHz communications, higher SCSs may be required due to the increased PN distortion and increased Doppler frequencies, which can be both partially mitigated through shorter multicarrier symbols. Additional important reason for increased SCS is the capability to achieve extremely high channel bandwidths with reasonable FFT size. Increasing the SCS leads also to reduced PHY latency, but it may also lead to some system design difficulties.

To address the above issues, the basic PHY numerology can be modified as shown in Table II. Inherited from Rel-15 NR, we assume that the supported SCSs still follow the scaling of 15 kHz with powers of two. Similar to Rel-15, we assume that FFT size of 4096 is used as baseline, and that the maximum number of physical resource blocks (PRBs) is 264, as currently defined in [8] for FR2. With 180 PRBs and 960 kHz SCS, the allocation bandwidth is 2.07 GHz which conforms well to the 2.16 GHz channel bandwidth, equaling the IEEE wireless local area network (WLAN) 802.11ay channel spacing [9].

The achievable PHY bit rates with maximum allocations and different modulations are shown in Table II. The bit rates are obtained by considering a rank-1 transmission with a slot of 14 OFDM symbols, of which one is reserved for physical downlink control channel (PDCCH) and one for demodulation reference signal (DMRS). In addition, PTRS overhead of 48 subcarriers corresponding to some 1.5% is assumed. This example shows that to reach larger than 10 Gb/s PHY bit rate, at least 2 GHz of bandwidth per operator should be considered.

While the support for increased SCS is important, use of lower SCS can also be desirable for several reasons. Firstly, it allows supporting longer CP length in time, alleviating synchronization and beam switching procedures. Secondly, it provides higher power spectral density (PSD) for transmitted signals with equal number of subcarriers. Thirdly, it decreases the sampling rates required by the UE, thus enabling reduced power consumption and higher coverage. Further, use of lower SCS enables support for users with lower bandwidth capabilities. Moreover, increasing the supported channel bandwidth with increased SCSs leads to increased transmitter (TX) distortion and RX noise power which limit the system coverage.

C. Relation to IEEE WLAN 802.11ay

The IEEE WLAN 802.11ay, and its predecessor 802.11ad, are important references for wireless communications at 60 GHz band [9], [10]. Although the system requirements, such as coverage and mobility support, are completely different, the need for power-efficient physical layer is of common

TABLE II: Physical layer numerology for 5G NR Rel-15 and corresponding numerology considerations for beyond 52.6 GHz communications. For reference, also an example of the 802.11ay numerology assuming normal guard interval and channel bonding of four 2.16 GHz channels is shown.

Parameter	**Value**											
	5G NR Rel-15 DFT-s-OFDM & OFDM				**Beyond 52.6 GHz Evolution DFT-s-OFDM & OFDM**						**802.11ay**	
											SC	**OFDM**
SCS [kHz]	15	30	60	120	**120**	240	480	960	1920	3840	3437.5	5156.25
Sampling freq. [MHz]	61.44	122.88	245.76	491.52	**491.52**	983.04	1966.08	3932.16	7864.32	15728.64	7040	10560
Slot duration [us]	1000	500	250	125	**125**	62.5	31.25	7.8125	3.90625	1.953125	-	
FFT size	4096				4096						2048	
Number of SCs per PRB	12				12						-	
Max. number of PRBs	270	273	264	264	264						-	
Max. allocation BW [MHz]	48.6	98.28	190.08	380.16	**380.16**	760.32	1520.64	3041.28	6082.56	12165.12	6160	8306.7
Max. channel BW [MHz]	50	100	200	400	**400**	800	1600	3200	6400	12800	8640	8640
PHY bit rate, QPSK [Gb/s]	0.1	0.2	0.3	0.6	**0.6**	1.2	2.4	4.8	9.6	19.2	12.29	13.27
PHY bit rate, 16-QAM [Gb/s]	0.2	0.3	0.6	1.2	**1.2**	2.4	4.8	9.6	19.2	38.3	24.57	26.54
PHY bit rate, 64-QAM [Gb/s]	0.2	0.5	0.9	1.8	**1.8**	3.6	7.2	14.4	28.8	57.5	49.15	53.08
PHY bit rate, 256-QAM [Gb/s]	0.3	0.6	1.2	2.4	**2.4**	4.8	9.6	19.2	38.3	76.7	-	-

interest. In 802.11ay, the single-carrier (SC) support is mandatory while the OFDM support is optional. It is also noted that in 802.11ay, the SC mode assumes utilizing a known Golay sequence as a guard interval between SC data symbol blocks, where the total length of data symbol block together with the guard interval corresponds to the used FFT size. Thus, 802.11ay SC can be considered as a unique word DFT-s-OFDM, instead of the cyclic prefix approach of 5G NR.

The physical layer of 802.11ay is clearly simpler than 5G NR, supporting only a single SCS, limited number of modulation and coding schemes, and clearly lower requirements on the link reliability. The FFT size of 512 is used to support channel bandwidth of 2.16 GHz, which can be extended with channel bonding up to maximum contiguous bandwidth of 8.64 GHz. Channel bonding refers to increased FFT size to provide larger channel bandwidth with the fixed SCS. Therefore, for 5G NR evolution to provide comparable instantaneous PHY bit rates with WLAN 802.11ay technology, channel bandwidths up to 8.64 GHz should be supported. For reference, the basic 802.11ay numerology is also shown in Table II. For the rank-1 PHY bit rates, we have assumed a continuous transmission burst of 2 ms, corresponding to the maximum physical layer convergence protocol data unit duration, and included the overhead of different training or channel estimation fields, headers, and interframe space between bursts.

IV. Phase Noise Challenge and PTRS Designs

A. Phase Noise Fundamentals

Phase noise refers to the random phase fluctuations of the RF oscillators, with good overview available in [7]. With OFDM and DFT-s-OFDM, PN causes a common phase error (CPE) which affects all the subcarriers within a multicarrier symbol similarly [11]. This means that only a single complex coefficient is required for CPE compensation. However, due to the relatively wide PSD of PN at mmWaves [7], it also causes inter-carrier interference (ICI) [11]. ICI can be mitigated by increasing the SCS, or by applying PTRS designs which allow for the estimation and compensation of the ICI components.

There are different PN models defined in 3GPP [12], building on current trends in phase-locked loops (PLLs). In general, there are two different local oscillator (LO) strategies for carrier frequency generation. In centralized LO approach, a single PLL is shared by all the RF transceivers, while in distributed carrier generation there are individual PLLs per each RF transceiver. All the evaluations in this paper are based on the centralized approach, i.e., there is only one PLL shared by all involved transceivers. This is a practical but also the worst-case assumption, performance-wise, because distributed carrier generation would give some phase noise averaging gain when the signals are combined in the receiver from different antenna ports.

Specifically, we assume the centralized LO PN model defined in [12, Section 6.1.11], which considers complementary metal oxide semiconductor (CMOS) based design for the UE due to lower cost and power consumption, and Gallium Arsenide (GaAs) based design for the BS. The power consumption of the UE model is 50 mW and for the BS it is 80 mW, and the loop bandwidth for the PLL-based PN models is 187 kHz for UE and 112 kHz for BS.

B. PTRS Designs of Rel-15 5G NR

1) Design for OFDM: With OFDM, individual PTRS symbols are inserted in frequency-domain with predefined frequency gap, as illustrated in Fig 1 (a), where the physical downlink shared channel (PDSCH) carries the DL user data. Thus, the OFDM PTRS structure relies on a distributed approach, occupying individual subcarriers with predefined distance. Rel-15 supports inserting PTRS to every second or fourth PRB in frequency-domain. Since PN varies rapidly over time, PTRSs need to be inserted densely in time. Therefore, every Lth OFDM symbol, where $L \in \{1, 2, 4\}$, can contain a PTRS. In the numerical evaluations, we assume the maximum density for Rel-15 PTRS which leads to overhead of $1/(2 \times 12) = 4.2\%$. Distributed frequency-domain insertion means that only CPE can be accurately estimated and compensated for each OFDM symbol containing PTRS, significantly limiting the performance with lower SCS or high-order modulations, as will be shown in Section V.

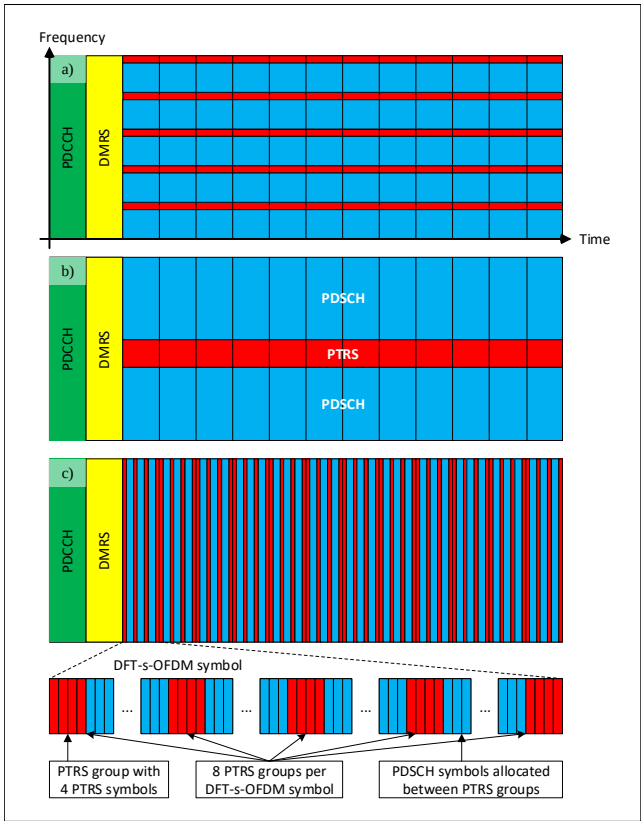

Fig. 1: Illustration of Rel-15 NR PTRS structures for (a) OFDM and (c) DFT-s-OFDM. In addition, the considered novel block PTRS structure for OFDM is illustrated in (b).

In the RX, after channel estimation and equalization, one can calculate the rotation of each PTRS in each OFDM symbol and average these to obtain CPE estimate, and finally compensate it before detection and decoding. Furthermore, CPE estimates for OFDM symbols without PTRS are obtained by interpolating the available estimates in time, leading however to increased detection latency and buffering requirements.

2) Design for DFT-s-OFDM: In Rel-15 standardization work, two different methods to insert PTRSs for DFT-s-OFDM were considered: pre-DFT and post-DFT. The latter would basically enable exactly the same compensation mechanisms as with OFDM. However, the former one was accepted to specifications due to its lower PAPR and better PN compensation capabilities. Thus, reference symbols are inserted before DFT to enable sample-level time-domain PN tracking.

The Rel-15 NR defines different configurations for group-based time-domain PTRS, where either 2 or 4 samples per group are used, and 2, 4, or 8 groups per DFT-s-OFDM symbol are supported [13, Table 6.4.1.2.2.2-1]. Thus, the maximum number of PTRS resources per DFT-s-OFDM symbol is $8 \times 4 = 32$, which results in overhead of 1.5% per DFT-s-OFDM symbol when $12 \times 180 = 2160$ subcarriers are used. This configuration is used as a Rel-15 baseline in Section V.

The DFT-s-OFDM PTRS concept is illustrated in Fig. 1 (c) together with DFT-s-OFDM symbol-wise PTRS allocation assuming maximum PTRS configuration. As the PTRS symbols are distributed in time, the RX can track the time-varying PN within each DFT-s-OFDM symbol. In the RX, after the frequency-domain channel equalization, the signal is converted back to time-domain using inverse DFT, after which the PN can be estimated from the time-domain PTRS and compensated before detection and decoding. For example, one can calculate the mean rotation in each PTRS group and use a simple linear interpolation to get the estimated PN values between the time-domain PTRS groups. Importantly, this allows a computationally efficient implementation to track and compensate time-varying PN within a DFT-s-OFDM symbol, which is not possible with the Rel-15 NR distributed PTRS for OFDM.

C. New PTRS Designs for Beyond 52.6 GHz Communications

1) Block PTRS Design for OFDM: The concept of frequency-domain block PTRS is introduced in [11]. The idea is to allocate a frequency-contiguous block of PTRS symbols, as shown in Fig. 1 (b), which allows to estimate PN-induced ICI components at RX. As the current Rel-15 specification dictates a specific frequency resolution for distributed PTRS, it is possible that with block PTRS based design one can achieve better performance with lower reference signal overhead in wide channels using fullband allocations. The block PTRS could be directly allocated as multiples of PRBs, where each PRB contains 12 subcarriers, to simplify control. However, block PTRS can also be allocated even with subcarrier resolution to maximize spectral efficiency, as long as the used block-size is equal to or larger than the number of unknowns in the estimation process [11]. Block PTRS is inserted to each OFDM symbol, as the time-continuity of ICI components is typically not guaranteed, and thus interpolation is not possible. On the other hand, having block PTRS in each OFDM symbol supports highly efficient pipelined RX architecture.

In addition to PN-induced ICI, block PTRS allows to compensate also for the ICI induced by time-varying channel (Doppler) and is thus well-suited also for high-mobility communications where the residual Doppler effects might be significant. Also in low-mobility scenarios in beyond 52.6 GHz communications, as will be shown in Section V, block PTRS allows to improve the link performance with front-loaded designs (i.e., a single DMRS in the beginning of the slot), as the time-varying channel during the slot duration causes ICI. In the numerical evaluations a block PTRS of size 4 PRBs, or 48 subcarriers, is assumed leading to overhead of 2.2% when assuming $12 \times 180 = 2160$ active subcarriers, which is clearly less than with the Rel-15 NR PTRS.

2) PTRS Design Enhancements for DFT-s-OFDM: It is also important to study whether the Rel-15 NR maximum PTRS configuration is sufficient to tackle the increasing PN at higher frequencies, or can we obtain significant performance improvements by defining new configurations. To improve the PN estimation capability with DFT-s-OFDM there are two options: 1) increasing the number of PTRS symbols per group, or 2) increasing the number of PTRS groups within the DFT-s-OFDM symbol. First approach provides averaging gain against noise and interference, and does not directly improve our capability to estimate fastly changing PN. Therefore, our proposal for the enhanced DFT-s-OFDM PTRS design focuses on increasing the number of PTRS groups, to allow improved

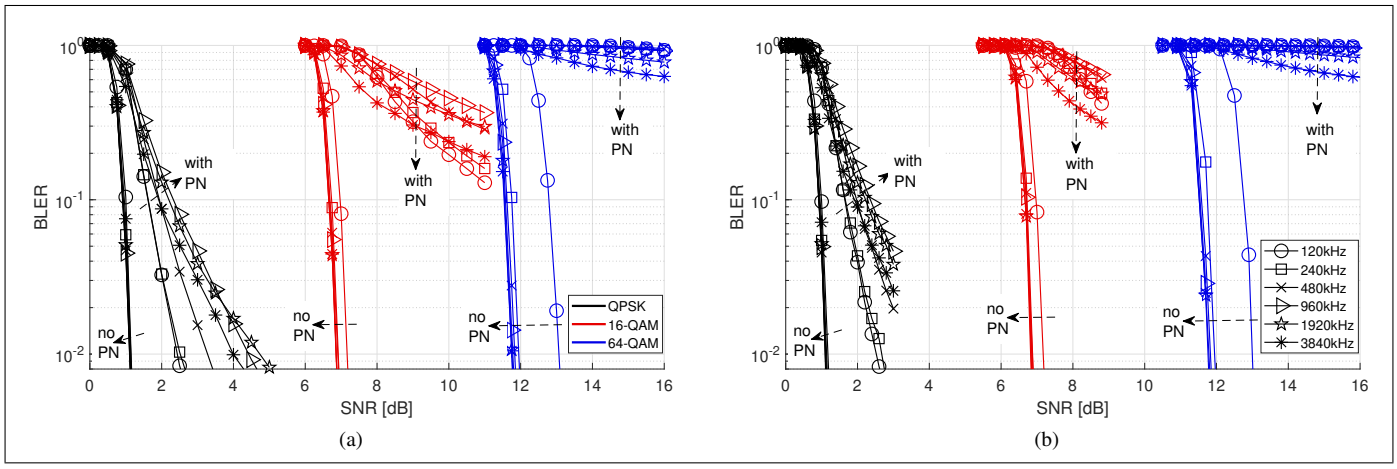

Fig. 2: Example radio link performance with and without PN when using (a) OFDM (b) DFT-s-OFDM. No PTRS based compensation is yet considered.

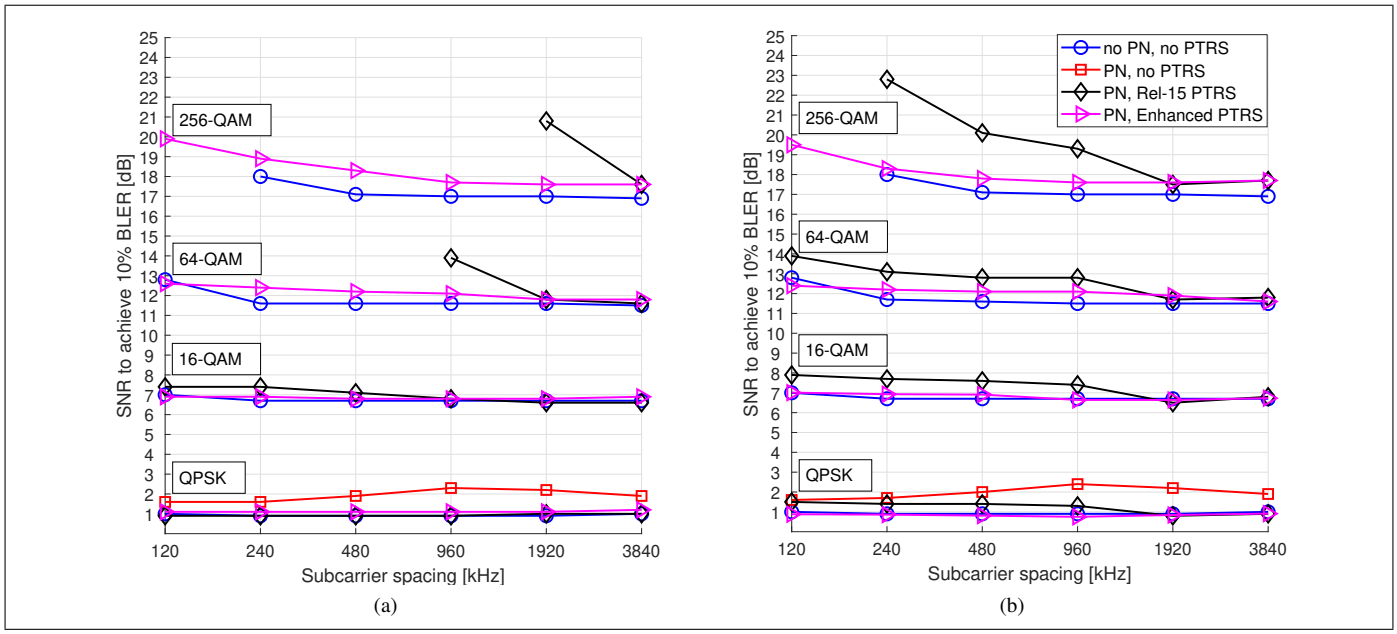

Fig. 3: Required SNR to achieve 10% block-error rate target at 60 GHz with different subcarrier spacings for a) OFDM and b) DFT-s-OFDM.

PN tracking within DFT-s-OFDM symbols. Detailed optimization is outside the article scope, and thus a design leading to the same overhead as the block PTRS proposed for OFDM is selected. Thus, we propose a new PTRS configuration for DFT-s-OFDM using 12 PTRS groups with four PTRS symbols per group, which results in 2.2% overhead when assuming 2160 active subcarriers.

V. Radio Link Performance at 60 GHz

The performance of OFDM and DFT-s-OFDM waveforms with or without PTRS and with or without PN distortion is evaluated over the selected SCS values shown in Table II and discussed in Section III. We assume a maximum channel bandwidth of 2.16 GHz, which follows the channelization for WLAN 802.11ay operating in 60 GHz unlicensed band [9]. Therefore, the maximum allocation size is limited to 180, 90, or 45 PRBs with SCSs of 960 kHz, 1920 kHz, or 3840 kHz, respectively. To obtain comparable performance with smaller SCS, we limit the maximum allocation size to 180 PRBs also with SCSs less than 960 kHz.

The adopted PN model is described in Section IV-A, following the BS and UE models for TX and RX, respectively, as defined in [12, Section 6.1.11]. The evaluations assume DL rank-1 transmission with polarization-specific antenna panels in BS and UE. There are 128 antenna elements organized into an 8x16 antenna array per polarization at BS and 16 antenna elements organized into a 4x4 antenna array per polarization at UE. The link performance is evaluated with QPSK, 16-QAM, 64-QAM, and 256-QAM modulations with fixed coding rate of $R = 2/3$. 5G NR Rel-15 compliant LDPC channel code is used. The used channel model is clustered delay-line E (CDL-E) with 10 ns root-mean-squared (RMS) delay-spread and Rician factor K =15 dB [14]. In all cases, 3 km/h UE mobility is assumed.

A. Radio Link Performance Without PTRS

First, to illustrate the significant effect of PN in beyond 52.6 GHz communications, the performance without PTRS and with or without PN is shown in Fig. 2, for selected modulations. The PN-free results show that all the SCSs

provide similar link performance for both waveforms. With only 1 DMRS symbol per slot, the channel variation caused by Doppler during the 14 OFDM symbol slot starts to degrade the link performance of 64-QAM with 120 kHz SCS. As will be shown later, ICI compensation allows to alleviate this problem.When considering the PN effects, we note that QPSK modulation can be supported without PTRS with some 1 dB-2 dB SNR loss. In addition, 16-QAM could be used without PTRS at 60 GHz, but with significant SNR losses to achieve 10% block error rate (BLER), indicating the need for PN estimation and compensation already with lower-order modulations. High-order modulations, 64-QAM and 256-QAM, do not work at all without PTRS under PN, as observed also from Fig. 3. Full BLER curves for all modulations are available in the supplementary electronic materials.

B. Radio Link Performance With PTRS

Fig. 3 compares the link performance when the Rel-15 or enhanced PTRSs are used for PN compensation. The performance with or without PN and without PTRS are also provided for reference. The x-axis includes different subcarrier spacings, while the y-axis shows the required SNR to achieve 10% BLER, which is a typical operating point in adaptive modulation and coding for the first transmission. Throughout this section, with DFT-s-OFDM, we use either the time-domain CPE estimate or the interpolated PN estimate, depending on which gives the best result. With OFDM and Rel-15 PTRS, only CPE compensation is possible. With novel block PTRS allowing for both CPE and ICI estimation [11], a contiguous allocation of 4 PRBs at the middle of the band is adopted, and four PN frequency components from both sides of the DC are estimated and used in the PN compensation.

We first conclude that the performance of lower-order modulations, QPSK and 16-QAM, can be clearly improved with Rel-15 PTRS, although these are typically assumed to operate without PTRS. For QPSK, the use of PTRS gives approximately 1 dB-2 dB SNR gain. In addition, Fig. 3 (a) shows that Rel-15 OFDM PTRS can support 64-QAM if SCS $\geq$ 960 kHz is used. On the other hand, as shown in Fig. 3 (b), DFT-s-OFDM with Rel-15 PTRS performs significantly better with 64-QAM, allowing to use all considered SCSs. From Fig. 3 (a), we also note that OFDM with Rel-15 PTRS can support 256-QAM with SCS $\geq$ 1920 kHz, whereas DFT-s-OFDM with Rel-15 PTRS can support 256-QAM already with SCS 240 kHz. Nevertheless, it is clear that if Rel-15 PTRS designs are not updated for OFDM or DFT-s-OFDM, significant radio link performance degradation is expected with the largest currently supported SCS of 120 kHz. The results shown in Fig. 3 (a) and (b) indicate, that by directly extending 5G NR Rel-15 FR2 operation to 60 GHz, data modulations only up to 16-QAM can be supported with OFDM, while DFT-s-OFDM based downlink could support modulation orders up to 64-QAM.

Furthermore, Fig. 3 (a) shows that by using the novel block PTRS with OFDM improves the performance significantly when compared to Rel-15, and even 256-QAM can be supported with all evaluated SCSs. This highlights the need for block PTRS support with OFDM in beyond 52.6 GHz communications, especially if considering the extension of 5G NR Rel-15 FR2 operation to 60 GHz band, and also the dominance of PTRS designs allowing ICI compensation over CPE compensation. For DFT-s-OFDM, increasing the number of PTRS groups from 8 to 12 can improve the performance significantly. Specifically, the used 12 PTRS groups allow to support 256-QAM over all evaluated SCSs with even better link performance than OFDM using block PTRS. Thus, DFT-s-OFDM based downlink combined with new PTRS configurations would allow to support 256-QAM modulation if current Rel-15 NR FR2 operation is extended to 60 GHz band.

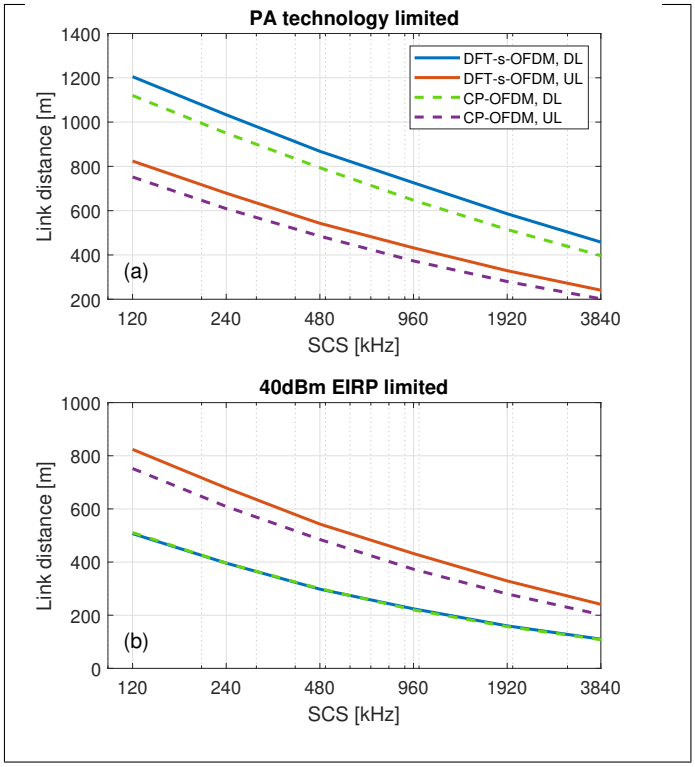

Fig. 4: Illustration of the achievable LOS link distance with CP-OFDM and DFT-s-OFDM assuming 16-QAM modulation in a) PA technology limited scenario and b) 40 dB EIRP limited scenario.

Related to the Doppler-induced ICI with 120 kHz SCS and front-loaded DMRS, Fig. 3 shows that with both waveforms the link performance degrades with 64-QAM, while 256-QAM does not anymore reach 10% BLER. With the enhanced PTRS designs, also this distortion is compensated, improving 64-QAM performance and enabling 256-QAM utilization with 120 kHz SCS. Additionally, with QPSK and 16-QAM, clear link performance improvements are observed with enhanced PTRS designs for both waveforms. In general, increasing SCS allows to tolerate more Doppler-spread and due to shorter multicarrier symbols, time-variant channel tracking is easier with fixed reference signal overhead.

VI. Link Budget Considerations for Beyond 52.6 GHz Communications

We finally consider link budget aspects for beyond 52.6 GHz communications, through the link budget tool that is available in the electronic materials. We assume urban-micro (UMi) LOS and UMi non-line-of-sight (NLOS) PL models [14, Table 7.4.1-1], while also consider the atmospheric gas attenuation

effects. We evaluate both EIRP-limited and PA technology limited scenarios, while consider full allocations for both DL and UL. In addition, 32 and 256 antenna elements are assumed for the UE and BS, respectively. 16-QAM modulation is considered, and the required SNR values are based on the results of Section V.

Building on [15], we consider 15.4 dBm as the PA saturation power available in BS and UE. Then considering the maximum power reduction required by 16-QAM [8, Table 6.2.2.1-2], the maximum PA output power per antenna element is 10.9 dBm with DFT-s-OFDM and 8.9 dB with CP-OFDM. Thus CP-OFDM provides a reduced maximum PA output power and link distance compared to DFT-s-OFDM. Therefore, supporting DFT-s-OFDM in DL would improve the BS power-efficiency because less power backoff is required and it could also enable the use of more non-linear PAs, leading to reduced costs. Furthermore, DFT-s-OFDM based downlink would allow using pulse-shaped $\pi/2$-BPSK modulation defined in 5G NR Rel-15 for further coverage extension.

Traditionally, the link distance is UL limited. This is observed also in Fig. 4 (a), where the link distance is limited by the PA output power and waveform specific maximum output power reduction. The DL link distance is clearly larger due to larger EIRP, while DFT-s-OFDM provides some 8 % and 10 % larger link distance in DL and UL, respectively. This gain is mainly due to the fixed PA technology assumption, which allows DFT-s-OFDM to achieve larger output power compared to OFDM.

However, the UL vs. DL situation can be drastically different at frequency bands where the same EIRP limit applies to both the BS and the UE. In Fig. 4 (b), the EIRP is limited to 40 dBm following the current regulation in Europe regarding unlicensed communications within 57 GHz–66 GHz [1, Table 4.2.2.1-2]. This leads to a scenario, where maximum EIRP in BS TX (corresponding to DL scenario) is achieved with smaller PA output power and therefore CP-OFDM and DFT-s-OFDM provide the same link distance results. On the other hand, due to the larger RX beamforming gain in the BS, the UL link distance is clearly larger, and dominated by the DFT-s-OFDM based waveform. Such DL-UL imbalance in EIRP-limited scenarios is often ignored in the system design or evaluation studies, and is thus here highlighted. It is also noted, that due to the given assumptions, the UL results for CP-OFDM and DFT-s-OFDM are identical in the EIRP-limited and PA technology limited scenarios.

VII. Conclusions

In this paper, the 5G NR technology evolution to beyond 52.6 GHz bands was discussed, with specific emphasis on physical layer numerology, phase noise challenges and comparison of OFDM and DFT-s-OFDM waveforms. Specifically, the performance and limitations of the current PTRS designs of 5G NR Rel-15 standard were evaluated and compared to the enhanced structures, which include a novel block PTRS design for OFDM and improved PTRS configurations for DFT-s-OFDM.

Through extensive performance evaluations, it was demonstrated that DFT-s-OFDM performs significantly better than OFDM when using Rel-15 PTRS structures. Furthermore, it was shown that even QPSK performance can be improved using PTRS, and that the proposed enhanced PTRS designs can support up to 256-QAM with all the evaluated subcarrier spacings up to 3840 MHz. Therefore, the existing Rel-15 FR2 solutions can be extended to 60 GHz and beyond if new block PTRS design is introduced for OFDM, or DFT-s-OFDM based downlink with new PTRS configurations is introduced for user data, while substantially larger channel bandwidths and thus larger bit rates and reduced latencies are available through the new increased SCSs.

References

[1] "3GPP TR 38.807 V1.0.0, "Study on NR beyond 52.6 GHz," Tech. Spec. Group Radio Access Network, Rel. 16," Oct. 2019.

[2] H. Holma, A. Toskala, and T. Nakamura, *5G Technology: 3GPP New Radio*. Wiley, 2019.

[3] M. Shafi *et al.*, "5G: A tutorial overview of standards, trials, challenges, deployment, and practice," *IEEE J. Sel. Areas Commun.*, vol. 35, no. 6, pp. 1201–1221, Jun. 2017.

[4] S. Shakib, J. Dunworth, V. Aparin, and K. Entesari, "mmWave CMOS Power Amplifiers for 5G Cellular Communication," *IEEE Communications Magazine*, vol. 57, no. 1, pp. 98–105, January 2019.

[5] S. Parkvall, E. Dahlman, A. Furuskar, and M. Frenne, "NR: The new 5G radio access technology," *IEEE Communications Standards Magazine*, vol. 1, no. 4, pp. 24–30, Dec. 2017.

[6] "3GPP TS 38.300 v. 15.9.0, "NR; NR and NG-RAN Overall Description; Stage 2," Tech. Spec. Group Radio Access Network, Rel. 15," June 2020.

[7] T. H. Lee and A. Hajimiri, "Oscillator phase noise: a tutorial," *IEEE Journal of Solid-State Circuits*, vol. 35, no. 3, pp. 326–336, March 2000.

[8] "3GPP TS 38.101-2 v. 16.0.0, "User Equipment (UE) radio transmission and reception; Part 2: Range 2 Standalone," Tech. Spec. Group Radio Access Network, Rel. 16," June 2019.

[9] P. Zhou *et al.*, "IEEE 802.11ay-Based mmWave WLANs: Design Challenges and Solutions," *IEEE Commun. Surv. Tut.*, vol. 20, no. 3, pp. 1654–1681, thirdquarter 2018.

[10] Y. Ghasempour, C. R. C. M. da Silva, C. Cordeiro, and E. W. Knightly, "IEEE 802.11ay: Next-generation 60 GHz communication for 100 Gb/s Wi-Fi," *IEEE Commun. Mag.*, vol. 55, no. 12, pp. 186–192, 2017.

[11] V. Syrjälä, T. Levanen, T. Ihalainen, and M. Valkama, "Pilot Allocation and Computationally Efficient Non-Iterative Estimation of Phase Noise in OFDM," *IEEE Wireless Commun. Lett.*, vol. 8, no. 2, pp. 640–643, Apr. 2019.

[12] "3GPP TR 38.803 v. 14.2.0, "Study on New Radio (NR) Access Technology; RF and co-existence aspects," Tech. Spec. Group Radio Access Network, Rel. 14," Sept. 2017.

[13] "3GPP TS 38.211 v. 15.8.0, "NR; Physical channels and modulation," Tech. Spec. Group Radio Access Network, Rel. 15," Dec. 2019.

[14] "3GPP TR 38.901 V15.1.0, "Study on channel model for frequencies from 0.5 to 100 GHz," Tech. Spec. Group Radio Access Network," Sept. 2019.

[15] K. Wu, K. Lai, R. Hu, C. F. Jou, D. Niu, and Y. Shiao, "77-110 GHz 65-nm CMOS Power Amplifier Design," *IEEE Transactions on Terahertz Science and Technology*, vol. 4, no. 3, pp. 391–399, May 2014.

BIOGRAPHIES

Toni Levanen is a post-doctoral researcher at Tampere University, Finland. His current research interests include physical layer design for 5G NR, interference modeling in 5G cells, and high-mobility support in mmWave communications.

Oskari Tervo received the D.Sc. (Tech.) degree from University of Oulu, Finland, in 2018 with distinction. He is currently working in Nokia Bell Labs, Oulu. His current research interests include physical layer aspects for cellular standardization.

Kari Pajukoski is a Fellow at Nokia Bell Labs, Finland. His research interests include cellular standardization, link and system simulation, and algorithm development.

Markku Renfors is a Professor Emeritus at Tampere University, Finland. His research interests are related to signal processing in wireless communications systems.

Mikko Valkama is a Full Professor at Tampere University, Finland. His research interests include radio communications, radio systems and signal processing, with specific emphasis on 5G and beyond mobile networks.